Quaternary Science Reviews 146 (2016) 238–250

Contents lists available at ScienceDirect

Quaternary Science Reviews

journal homepage: www.elsevier.com/locate/quascirev

Teleconnected ocean forcing of Western North American droughts and pluvials during the last millennium

Cody C. Routson [a, *], Connie A. Woodhouse [b, c, d], Jonathan T. Overpeck [b, e, f], Julio L. Betancourt [g], Nicholas P. McKay [a]

[a] School of Earth Sciences and Environmental Sustainability, Northern Arizona University, Flagstaff 86011, AZ, USA
[b] Department of Geosciences, University of Arizona, Tucson, AZ 85721, USA
[c] Laboratory of Tree-Ring Research, University of Arizona, Tucson, AZ 85721, USA
[d] School of Geography and Development, University of Arizona, Tucson, AZ 85721, USA
[e] Institute of the Environment, University of Arizona, Tucson, AZ 85721, USA
[f] Department of Atmospheric Sciences, University of Arizona, Tucson, AZ 85721, USA
[g] National Research Program, Water Mission Area, U.S. Geological Survey, Reston, VA 20192, USA

ARTICLE INFO

Article history:
Received 27 January 2016
Received in revised form
22 June 2016
Accepted 23 June 2016
Available online 6 July 2016

Keywords:
Western North America
Drought
Pluvial
Synthesis
Climate change
Multi-proxy

ABSTRACT

Western North America (WNA) is rich in hydroclimate reconstructions, yet questions remain about the causes of decadal-to-multidecadal hydroclimate variability. Teleconnection patterns preserved in annually-resolved tree-ring reconstructed drought maps, and anomalies in a global network of proxy sea surface temperature (SST) reconstructions, were used to reassess the evidence linking ocean forcing to WNA hydroclimate variability over the past millennium. Potential forcing mechanisms of the Medieval Climate Anomaly (MCA) and individual drought and pluvial events—including two multidecadal-length MCA pluvials—were evaluated. We show strong teleconnection patterns occurred during the driest (wettest) years within persistent droughts (pluvials), implicating SSTs as a potent hydroclimate forcing mechanism. The role of the SSTs on longer timescales is more complex. Pacific teleconnection patterns show little long-term change, whereas low-resolution SST reconstructions vary over decades to centuries. While weaker than the tropical Pacific teleconnections, North Atlantic teleconnection patterns and SST reconstructions also show links to WNA droughts and pluvials, and may in part account for longer-term WNA hydroclimate changes. Nonetheless, evidence linking WNA hydroclimate to SSTs still remains sparse and nuanced—especially over long-timescales with a broader range of hydroclimatic variability than characterized during the 20th century.

1. Introduction

Annually resolved tree-ring records have shown that Western North America (WNA) has experienced a wide range of hydroclimatic conditions over the past millennium. Most remarkable has been the occurrence of megadroughts: multidecadal-length droughts more persistent than any observed during the instrumental record (Woodhouse and Overpeck, 1998). Megadroughts, defined as prolonged drought lasting more than two decades, occurred throughout the last millennium, but were more frequent during the Medieval Climate Anomaly (MCA, ~900–1400 AD), (Cook et al., 2004, 2007, 2010b; Meko et al., 2007; Routson et al., 2011; Woodhouse and Overpeck, 1998). Multidecadal-length pluvials, or megapluvials, are also documented throughout the last millennium, but have received less attention than megadroughts despite their comparable societal importance. Here, we reassess the evidence linking these past WNA megapluvials and megadroughts to global sea surface temperature (SST) variations.

Observational records (up to ~100 years), document strong causal linkages known as teleconnections between SSTs and WNA climate (e.g., Cayan et al., 1999; Cook et al., 2010a,b; Kam et al.,

Abbreviations: WNA, Western North America; SST, Sea Surface Temperature; MCA, Medieval Climate Anomaly; ENSO, El Niño Southern Oscillation; PDO, Pacific Decadal Oscillation; AMO, Atlantic Multidecadal Oscillation; NAM, Northern Hemisphere annular mode; PDSI, Palmer Drought Severity Index; NADA, North American Drought Atlas.

* Corresponding author. PO Box 4099, 625 S Knoles Dr, Building 12, Rm 100, Flagstaff, AZ 86011-4099, USA.
E-mail address: Cody.Routson@nau.edu (C.C. Routson).

http://dx.doi.org/10.1016/j.quascirev.2016.06.017
0277-3791/

2014; McCabe et al., 2004, 2008; Tootle et al., 2005; Wang and Mehta, 2008). Because ocean-driven SSTs have a longer memory or persistence than the atmosphere alone, SST variability is the most likely cause of persistent multidecadal-to-centennial hydroclimate variability. WNA climate is strongly connected to SSTs in the tropical Pacific, as characterized by the impact of the El Niño Southern Oscillation (ENSO) (Redmond and Koch, 1991). During La Niña events, cool conditions in the eastern equatorial Pacific tend to displace westerly, mid-latitude, storm tracks northward, resulting in reduced cool season precipitation in southwestern North America (e.g., Cayan et al., 1999; Redmond and Koch, 1991; Schubert et al., 2009). The opposite tends to be true for El Niño events. Persistent ENSO conditions have been linked to decadal-scale WNA hydroclimate variability over the past ~150 years (Seager et al., 2005). On decadal to multidecadal timescales, the Pacific Decadal Oscillation (PDO) reflects the dominant mode of SST in the North Pacific (Mantua et al., 1997). Linked with tropical Pacific variability (Newman et al., 2003), the PDO also has demonstrated connections with WNA climate (McCabe et al., 2004, 2008; Tootle et al., 2005). The Indian Ocean works in concert with the Pacific whereby warming in the western Pacific and Indian oceans drives deep atmospheric convection that influences the rising limb of the Walker Cell, and ultimately affecting the mean position of storm tracks and WNA cool season rainfall (Wang and Mehta, 2008). ENSO, PDO, and Indian Ocean all tend to modulate anti-phased precipitation in a well-known dipole between southwestern (Southwest) and northwestern North America (Northwest).

North Atlantic SSTs, as characterized by the Atlantic Multidecadal Oscillation (AMO), may also influence WNA drought, although less directly and to a lesser degree than the Pacific (Cook et al., 2010a,b; Feng et al., 2010; Kam et al., 2014; McCabe et al., 2004; McCabe and Wolock, 2013; Schubert et al., 2009; Tootle et al., 2005). Warm North Atlantic SSTs are associated with warmer WNA temperatures. Regional warming associated with a positive AMO was shown to decrease runoff efficiency and streamflow in the Upper Colorado River Basin (Nowak et al., 2012). The impact of the North Atlantic may not be limited, however, to regional temperature effects on the water cycle (Feng et al., 2010; Kam et al., 2014; McCabe et al., 2004; Schubert et al., 2009). Pacific forcing appears to influence atmospheric circulation patterns driven by the AMO during some seasons (Hu and Feng, 2012). Instrumental records and climate models also suggest the largest precipitation anomalies in WNA tend to occur when Pacific and Atlantic SSTs are opposite in sign (Feng et al., 2010; Kam et al., 2014; McCabe et al., 2004, 2008; Schubert et al., 2009), reflecting a combined influence of ocean basins on global atmospheric circulation.

The inference that past megadroughts were caused by an extension or enhancement of the processes influencing WNA climate today is prevalent in the literature, although the proposed mechanisms driving this inference vary. The predominant hypothesis is that tropical Pacific SSTs drove sustained WNA aridity, in which extended La Niña-like conditions forced medieval megadroughts (e.g., Conroy et al., 2009a; Graham et al., 2007; Herweijer et al., 2007; Seager et al., 2007; Stahle et al., 2000). Links also have been drawn between the AMO and past WNA drought over the past ~500 years as established by tree rings (Gray et al., 2004; Hidalgo, 2004). North Atlantic SSTs are less well-constrained before ~1500 AD, but some SST proxy records indicate tenuous multidecadal to centennial-scale relationships between North American climate and the North Atlantic (Conroy et al., 2009a; Feng et al., 2008, 2010; Oglesby et al., 2012).

Various general circulation model studies support the paleoclimatic evidence and interpretations for the causes of megadroughts. A cool tropical Pacific has been shown to simulate WNA megadroughts in several studies (Burgman et al., 2010; Graham et al., 2007; Seager et al., 2008), and some modeling results indicate a warm North Atlantic plays a role in modulating drought in the Southwest and Midwest (e.g., Feng et al., 2010; Oglesby et al., 2012). Some evidence suggests that ocean teleconnections with recent North American droughts may be weakening, while atmospheric teleconnections are strengthening (Kam et al., 2014; Kumar et al., 2013; Seager et al., 2014; Wang et al., 2014). Though this recent shift may be related to greenhouse warming, it is conceivable that similar shifts, from oceanic to atmospheric controls of North American droughts and pluvials, also have happened in the past.

Traditionally, most paleoclimatic studies have focused on the causes of WNA megadroughts over megapluvials, and have not fully evaluated the associations of both to global SST anomalies over past millennium. For example, because background conditions may vary at longer time scales, the drivers for two known pluvials embedded in the generally droughty period of the MCA could differ substantially from those during the wetter post-MCA. Here we extend previous work, using a multiproxy approach to assess the evidence linking SSTs to persistent wet and dry periods in WNA over the past millennium. We use teleconnection patterns embedded in gridded drought reconstructions (Cook and Krusic, 2008), and a screened network of global SST proxy records to explore the following research questions:

1) Are differences in WNA hydroclimate between the MCA and post-MCA linked to SSTs?
2) What evidence links WNA megadroughts and megapluvials to SST forcing during the past millennium?
3) Do SST/pluvial associations vary with multidecadal variability, for example, within the MCA?

2. Materials and methods

2.1. Defining droughts and pluvials

Droughts and pluvials over the period 900–2006 AD were characterized with the North American Drought Atlas (NADA, Cook and Krusic, 2008). The NADA is a gridded network of tree-ring reconstructed drought as defined by the Palmer Drought Severity Index (PDSI, Palmer, 1965). Although the NADA reconstructed drought metric is summer season PDSI (Cook et al., 2004), tree rings have inherent seasonal climate sensitivities, and for this reason, the WNA portion of the NADA used here primarily reflects winter precipitation (St. George et al., 2010). PDSI grid points used for WNA (27.5°N to 50° N, 97.5°W to 125°W, after Cook et al., 2004) were averaged and smoothed with a 50-year cubic smoothing spline to highlight regional multidecadal variability (Fig. 1). Pluvial and drought periods were identified as intervals during which the smoothed series exceeded 0.2 PDSI units above or below the series mean (−0.17) respectively. This threshold was chosen qualitatively as one that encompasses all relatively severe droughts and pluvials with low frequency components that persisted for multiple decades. We also looked at two subset regions, the Southwest and Northwest (32°N to 40° N, 105°W to 115°W and 42°N to 50° N, 110°W to 125°W, respectively, after Cook et al., 2014) for comparison of droughts and pluvials.

2.2. Teleconnection patterns

Correlation maps were used to investigate relationships between drought and pluvial patterns and the teleconnections documented by circulation modes. First, instrumental circulation

indices for December–February were correlated with each gridpoint in the NADA to develop modern teleconnection pattern maps. The December–February season was used because the teleconnections tend to be strongest in the cool season, which also coincides with the seasonality of the WNA tree-ring reconstructed PDSI (St. George et al., 2010). The circulation indices used were the NINO3 index (1856–2006; EXTENDED NINO3 index: Kaplan et al., 1998; Reynolds et al., 2002), the PDO index (1900–2006; Mantua et al., 1997) and the AMO index (1880–2006; van Oldenborgh et al., 2010). The modern teleconnection pattern maps were then spatially correlated with the gridded reconstructed PDSI for every year in the 900–2006 AD analysis period. This resulted in WNA teleconnection pattern strength time series for each of three circulation indices. For example, for NINO3, the time series reflects the strength of the relationship between the modern ENSO/drought spatial pattern and spatial pattern of drought for each year of reconstructed gridded PDSI; the time series is the correlation between the two patterns for each year. Both the modern teleconnection maps and their spatial correlations with gridded PDSI over the past millennia were developed by using the entire set of North American gridded PDSI, not the just subset used to define Western droughts and pluvials. We assessed the teleconnection time series during pluvials and droughts (as defined above, based on smoothed WNA time series), and for the individual wet years and dry years within pluvials and droughts. The wet and dry years were defined by unsmoothed WNA average PDSI deviations exceeding ±1 respectively (e.g., Cook et al., 2007).

An important caveat of this method should be noted: because teleconnection patterns are non-stationary (e.g., Batehup et al., 2015; Cole and Cook, 1998; Hu and Feng, 2001; McCabe and Dettinger, 1999), this method produces only a rough estimate of the association between these modes of circulation and past WNA climate variability. The goal here is to document variability in the strength of the teleconnections over time, not to reconstruct the respective circulation modes. The teleconnection patterns themselves may be generally indicative of the role of Pacific and Atlantic SSTs, particularly at the spatial scale considered here, and used to help assess potential SST forcing mechanisms of WNA drought variability.

2.3. Spectral analysis

We calculated power spectra, by using the multitaper method (Thomson, 1982) on the tree-ring reconstructed PDSI and teleconnection time series, to test if low-frequency characteristics of the PDSI—that is the persistence of droughts and pluvials—during the MCA (e.g., Herweijer et al., 2007) can be attributed to changes in a particular teleconnection pattern and associated ocean basin. The series were normalized by their mean and variance and detrended prior to spectral analysis. The time series were split into MCA (900–1400 AD) and post-MCA (1400–2000 AD) segments. The 95% significance test for spectral peaks was developed by using a Monte Carlo approach: spectra were computed on 5000 random series with the same AR1 autocorrelation and variance as the original series. The upper 95th percentile for each distribution was used as the confidence limit for testing significance.

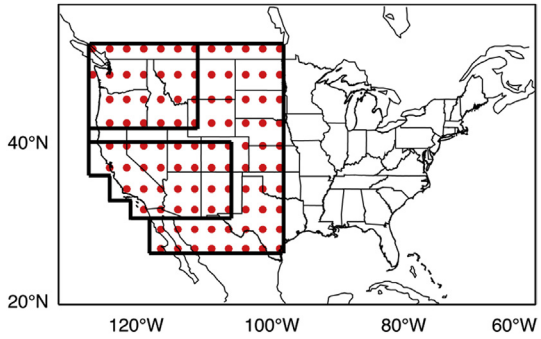

Fig. 1. Western North American PDSI reconstruction grid following Cook et al. (2004). The Northwest and Southwest grid subsets are denoted by the respective boxes following the regions used by Cook et al. (2014).

2.4. PaleoSST reconstruction anomaly maps

To further investigate links between WNA climate and SST forcing, we assessed proxy SST reconstructions. The SST reconstructions, based on marine proxy records, provide direct observations of the potential drought and pluvial forcing mechanisms. Although there are limitations with these records as discussed below, the SST reconstructions provide an independent test of ocean background conditions over long MCA to post-MCA timescales, and (albeit less reliably) during multidecadal-scale drought and pluvial events.

The SST records were obtained from the Expanded Global Holocene Spatial and Temporal Climate Variability database (Leduc et al., 2010a), NOAA's paleoclimate database (http://www.ncdc.noaa.gov/paleo/paleo.html), the PANGEA data library (http://www.pangaea.de), or digitized from the publication when not in public repositories and when authors did not respond to our data requests. Proxy SST records were screened by resolution and age control. Records were retained with 20 or more data points in the analysis period, and two or more age control points in the analysis period (900–2006 AD). For the drought and pluvial analysis, records were retained with data points in at least two drought or two pluvial intervals, respectively. A total of 51 records passed the screening (Fig. 2. Table 1). To assess potential relationships between SSTs and past WNA climate, we evaluated proxy SST anomalies for MCA and post-MCA periods, and for drought and pluvial intervals. Proxy SST anomalies were computed with respect to the 900–2006 AD mean, or series length mean, if shorter than the analysis period.

It is important to note the limitations of using proxy SST reconstructions to assess ocean surface temperature patterns during drought and pluvial events. The first uncertainty is the seasonal dependency of some SST proxies (e.g., Leduc et al., 2010a), whereby the seasonality's the SST proxies are not necessarily aligned with those of the circulation modes. A second limitation is that the SST proxy resolution is lower, with greater dating uncertainty, than the tree-ring reconstructed PDSI. Thus, the proxy SST reconstructions reflect variability over long time-scales (decadal to centennial), whereas tree-ring records preserve predominantly annual-to-decadal-scale variability (e.g., Cook et al., 1995). Consequently, the SST anomaly maps are not reflecting the same time-scales of variability as the tree-ring drought records, and assessing the influence of SST anomalies for relatively short, individual drought and pluvial intervals is unlikely to provide meaningful constraints. To help alleviate the resolution and dating uncertainty mismatch, we analyzed a composite of all drought and pluvial intervals to average out some dating uncertainty in the SST records and assess general relationships. Nonetheless, the proxy SST anomaly maps characterize long-term (multi-century scale) changes in the oceans, and droughts and pluvials that are driven by relatively short term anomalies in SST patterns will not be apparent in this analysis.

2.5. Additional evidence

We employ several other sources of evidence of past WNA drought and pluvial forcing mechanisms, including several tropical

precipitation reconstructions as indicators of tropical Pacific SST variability. We also evaluate the dominant modes of the NADA as characterized by Woodhouse et al. (2009), to assess the potential causes of the MCA pluvials. They defined two dominant modes of North American drought by using principal components analysis, that are linked to ENSO and the Northern Hemisphere annular mode (NAM) respectively.

3. Results

3.1. Drought and pluvial events

Smoothed WNA PDSI characterizes seven persistent droughts and eight persistent pluvials between 900 and 2000 AD (Fig. 3a, Table 2). The WNA droughts occurred predominantly in the MCA whereas pluvials were more concentrated in the post-MCA period. Two persistent WNA pluvials, however, occurred in the MCA and two persistent droughts occurred in the post-MCA. The widespread drought and pluvial events primarily reflect events that span WNA, including regions with somewhat different (and sometimes opposing) teleconnections. Pluvials and droughts for the Northwest and Southwest show strong coherence through the MCA, but major differences after about 1400 (Fig. 3b and c). Whereas a number of the pluvials are shared in the two regions over the post-MCA period, the patterns of droughts are not. This suggests that large-scale drivers of pluvials and drought were dominant in the MCA, influencing the entire region in the same way, whereas regional-scale drivers were more important after this period. Because of this common variability on longer timescales, in this study we focused on westwide patterns of droughts and pluvials.

3.2. Teleconnection patterns

The teleconnection pattern maps documenting the correlations between instrumental circulation indices and North American PDSI are shown in Fig. 4a–c and are similar to those shown in Cook et al. (2014). The NINO3 and PDO teleconnection maps are characterized by a north-south dipole in WNA climate: when the Southwest is dry, the Northwest is wet and vice versa (Fig. 4a–b). The NINO3 teleconnection pattern is stronger and more widespread in the Southwest, whereas the PDO has a stronger signature in the Northwest. Nonetheless, spatial teleconnection patterns of the PDO and NINO3 in WNA are extremely similar. The modern relationship between the AMO and WNA climate is less pronounced. The AMO has a weakly negative but significant relationship with PDSI across much of North America during the instrumental period (Fig. 4c).

Correlating the teleconnection maps with the annual reconstructed NADA maps over the 900–2000 AD analysis period results in time series of r-values, indicating the strength and sign of the teleconnection patterns through time (Fig. 4d–f). The NINO3 teleconnection time series (Fig. 4d) ranges between $r = 0.81$ and $r = -0.80$ with a mean absolute teleconnection strength of $r = 0.32$. The PDO teleconnection time series (Fig. 4e) ranges between $r = 0.76$ and $r = -0.77$ with a mean absolute teleconnection strength of $r = 0.30$. Not surprisingly the PDO and NINO3 teleconnection time series are nearly identical to each other ($r = 0.96$, $p < 0.0001$), as reflected by their teleconnection patterns. As a result, distinguishing between the NINO3 and PDO patterns is not feasible. Correlations between the AMO teleconnection pattern and WNA PDSI are weaker (Fig. 4f), and range between $r = \pm 0.61$ with a mean absolute teleconnection strength of $r = 0.18$. The NINO3 and AMO teleconnection series are negatively correlated with each other ($r = -0.57$, $p < 0.0001$), as are the PDO and AMO teleconnection time series ($r = -0.57$, $p < 0.0001$). The NINO3 teleconnection series has the strongest relationship with WNA PDSI ($r = 0.77$), followed by the PDO teleconnection series (0.55) and the AMO teleconnection series (-0.43).

The teleconnection patterns are not markedly different in the MCA and Post-MCA in WNA. Negative (La Niña) NINO3 teleconnection patterns are slightly more frequent during the MCA (59% of all years) than the post MCA (53% of all years). The average absolute strength of the NINO3 teleconnection pattern series does not change between the MCA ($r_{abs} = 0.32$) and post-MCA ($r_{abs} = 0.31$). The frequency of positive/negative AMO teleconnection patterns changes slightly between the MCA and post MCA (positive AMO in 54% of all years during the MCA and 45% of all years in the post MCA). The average absolute AMO teleconnection pattern strength also increases during the MCA ($r_{abs} = 0.22$) with respect to the post-MCA ($r_{abs} = 0.14$).

Mean teleconnection patterns do not show strong differences between droughts and pluvials. During droughts, the teleconnection series strength averages for NINO3, PDO, and AMO are -0.11, -0.07, and 0.04, respectively. During pluvials, the values for NINO3, PDO, and AMO are 0.02, 0.03, and -0.04, respectively. However, persistent pluvials and droughts contain years that represent breaks in these persistent conditions. For example, the 12th century drought in the upper Colorado River Basin that persisted for six decades contained about a dozen above average flow years (Meko et al., 2007). NADA maps show that individual anomalous dry or wet years within decadal-scale droughts and pluvials respectively have much stronger teleconnection patterns than the overall events, suggesting that the teleconnection patterns

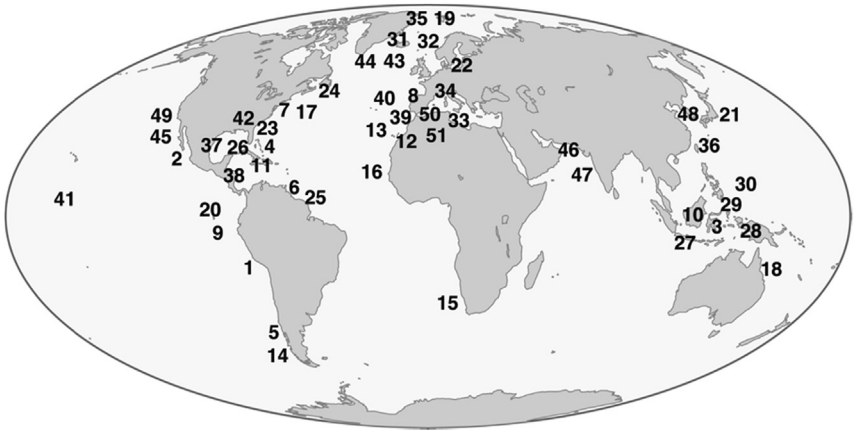

Fig. 2. Proxy sea surface temperature record site location key. Site numbers correspond with records in Table 1 and corresponding supplemental dataset.

Table 1
Proxy SST records including location, reference, resolution, and age control used in this analysis. Records are available in the associated supplemental dataset.

#	Core name	Reference	Lat (°N)	Lon (°E)	Resolution: mean (min max) yr/smpl	Proxy	Dating method	# of 14C	# of 210PB	Total tie points
1	B0406	Gutiérrez et al. (2011)	−14.13	−76.50	2.7 (1–7)	Alkenone	210Pb, AMS 14C	6	4	10
2	BC-43	Goni et al. (2006)	27.90	−111.66	4.6 (4–13)	Alkenone	210PB, varve		59	59
3	BJ8-03-32GGC	Oppo et al. (2009)	−3.53	119.27	10 (10–10)	Mg/Ca	210Pb, AMS 14C, Tephra	5.0	13.0	19.0
4	Bahamas Coral	Saenger et al. (2009)	25.84	−78.62	1 (1–1)	Coral	U/Th, annual growth bands			7 + band chron
5	CF7-PC33	Sepúlveda et al. (2009)	−44.33	−72.97	20.4 (8–49)	Alkenone	AMS 14C	4		4
6	PL07-73	Black et al. (2007)	10.75	−64.77	1.4 (0.5–2.6)	Mg/Ca	Varve, 210Pb, AMS 14C	12	30	42 + varve chron
7	MD99-2209	Cronin et al. (2003)	37.82	−76.12	3.2 (1–34.7)	Mg/Ca	137Cs, 210Pb, AMS 14C	9	Multiple Cores	9+
8	D13882	Rodrigues et al. (2009)	38.63	−9.45	22.4 (21–44)	Alkenone	AMS 14C	1		1
9	El Junco	Conroy et al. (2009b)	−0.90	−89.48	5.5 (1–9)	Diatom	137Cs, 210Pb, AMS 14C	4	9	14
10	GGC13	Linsley et al. (2010)	−7.40	115.20	33 (23–35)	Mg/Ca	AMS 14C	1		1
11	79GGC	Lund and Curry (2006)	24.36	−83.35	22.9 (9–104.8)	Mg/Ca	AMS 14C	3		3
12	GeoB6007-2	Kim et al. (2004)	30.85	−10.27	31.1 (31–32)	Alkenone	AMS 14C	1		1
13	GeoB6008-6	McGregor et al. (2007)	30.85	−10.10	7.9 (0.5–13)	Alkenone	210Pb, AMS 14C	3	15	18
14	GeoB71863	Mohtadi et al. (2007)	−44.15	−75.16	51.4 (19.2–99)	Alkenone	AMS 14C	3		3
15	GeoB8331-4	Leduc et al. (2010b)	−29.14	16.72	21.9 (19–33)	Alkenone	210Pb, AMS 14C	1	17	18
16	GeoB9501-5	Kuhnert and Mulitza (2011)	16.84	−16.73	9.4 (5–28)	Mg/Ca	AMS 14C	2		2
17	Gulf of Maine Shells	Wanamaker et al. (2007)	43.65	−69.80	3 (1–394)	Bivalves	Annual band counting, AMS 14C	3		3 + layer chron
18	Barrier Reef Coral	Hendy et al. (2002)	−18.33	146.45	5.1 (5–10)	Coral Sr/Ca	annual growth bands			band chron
19	JM-06-WP-04-MCB	Bonnet et al. (2010)	78.92	6.77	39.7 (15.3–85.6)	dinocyst taxa	137Cs, 210Pb, AMS 14C	2	9	12
20	KNR195-5	Rustic et al. (2015)	1.25	−89.69	45.4 (26.5–81)	Mg/Ca	AMS 14C	3		3
21	KR02-06A	Isono et al. (2009)	36.03	141.78	24.3 (11–53)	Alkenone	AMS 14C	3		3
22	M200309/ENAM9606	Richter et al. (2009)	55.65	13.99	17.4 (11–37)	Mg/Ca	226Ra, 137Cs, 210Pb, AMS 14C	4	13	17
23	118MC-A	Lund and Curry (2006)	24.59	−79.27	24.6 (22.5–25.7)	Mg/Ca	AMS 14C	2		2
24	MC-29D	Keigwin et al. (2003)	45.89	−62.80	26.8 (7.9–53)	Alkenone	210Pb, AMS 14C	2	11	13
25	MC4	Goni et al. (2006)	10.65	−64.66	7.7 (2–23)	Alkenone	210Pb, AMS 14C, varve			varve chron
26	62MC-A	Lund and Curry (2006)	24.33	−83.26	26.6 (11–50)	Mg/Ca	AMS 14C	2		2
27	MD98-2160	Newton et al. (2006)	−5.20	117.48	7.5 (1–20)	Mg/Ca	AMS 14C, Tephra	3		4
28	MD98-2176	Stott et al. (2004)	−5.00	133.44	27.2 (10–66)	Mg/Ca	AMS 14C	2		2
29	MD98-2177	Newton et al. (2011)	1.40	119.08	12.2 (10.9–21.8)	Mg/Ca	AMS 14C	2		2
30	MD98-2181	Stott et al. (2004)	6.30	125.82	19.7 (2–88)	Mg/Ca	AMS 14C	5		5
31	MD99-2275	Sicre et al. (2008); (2011)	66.56	−17.70	3.2 (1–6)	Alkenone	Tephra Chronology, 210pb		23	28
32	MD99-2275	Eiríksson et al. (2006)	66.56	−8.00	15.3 (3.3–27.2)	Diatom	AMS 14C, Tephra Chronology	7		11
33	MINMC06-1a	Moreno et al. (2012)	40.50	4.03	34.7 (11–70)	Alkenone + Mg/Ca	AMS 14C	4		4
34	MINMC06-1b	Moreno et al. (2012)	40.50	4.03	37.8 (11.7–70)	Alkenone + Mg/Ca	AMS 14C	4		4
35	MSM5/5-712	Spielhagen et al. (2011)	78.91	6.77	35.8 (18–54)	Forams	AMS 14C	3		3
36	ODP-1202B	Wu et al. (2012)	24.80	122.50	28.2 (13–104)	Tex86	AMS 14C	2		2
37	PE07-2	Richey et al. (2009)	26.68	−93.93	23.2 (11.8–33.1)	Mg/Ca	AMS 14C	3		3
38	PE07-5I	Richey et al. (2009)	27.55	−92.17	18.8 (18.8–8.8)	Mg/Ca	AMS 14C	3		3
39	PO287-26	Rodrigues et al. (2009)	38.33	−9.21	11.8 (3–85)	Alkenone	210Pb, AMS 14C	6	12	18
40	PO287-26-2	Abrantes et al. (2005)	38.56	−9.35	9 (1–161)	Alkenone	210Pb, AMS 14C	1		1 + cross correlation
41	Palmyra	Cobb et al. (2003)	6.00	−160.00	2.5 (1–189)	Coral	U/Th			25
42	PigmyBasin	Richey et al. (2007)	27.20	−91.42	13.3 (12.3–37)	Mg/Ca	AMS 14C	5		5 + varve chron
43	RAPid-21-3K	Sicre et al. (2011)	57.45	−27.91	10.4 (10–30)	Alkenone	AMS 14C	5		5 + varve chron
44	Rapid-21	Miettinen et al. (2012)	57.27	−27.54	5.6 (1–21)	Diatom	210Pb, AMS 14C	9	5	14
45	SABA8772 and SABA8871	Hendy et al. (2013); Zhao et al. (2000); Schimmelmann et al. (2013)	34.23	−120.02	1.2 (0.1–8.2)	Alkenone	AMS 14C and Varve	25		25 + varve chron
46	SO90-39KG	Doose-Rolinski et al. (2001)	24.83	65.92	16.5 (1–46)	Alkenone	Varve and AMS 14C	5		5 + varve chron
47	SO13-0275KL	Doose-Rolinski et al. (2001)	24.83	65.92	11.2 (6–29)	Alkenone	Varve and AMS 14C	5		5 + varve chron
48	SSDP-102	Kim et al. (2004)	34.95	128.88	45 (15–78)	Alkenone	AMS 14C	3		3
49	ODP893A	Kennett and Kennett (2000)	34.29	−120.04	28.8 (10.1–96.1)	Mg/Ca	AMS 14C	11		11
50	436B	Nieto-Moreno et al. (2013)	36.21	−4.31	30 (6–65)	Tex86, Alkenone, BIT	210Pb, AMS 14C	2	10	12
51	384B	Nieto-Moreno et al. (2013)	35.99	−4.75	38.9 (6–66)	Tex86, Alkenone, BIT	210Pb, AMS 14C	2	10	12

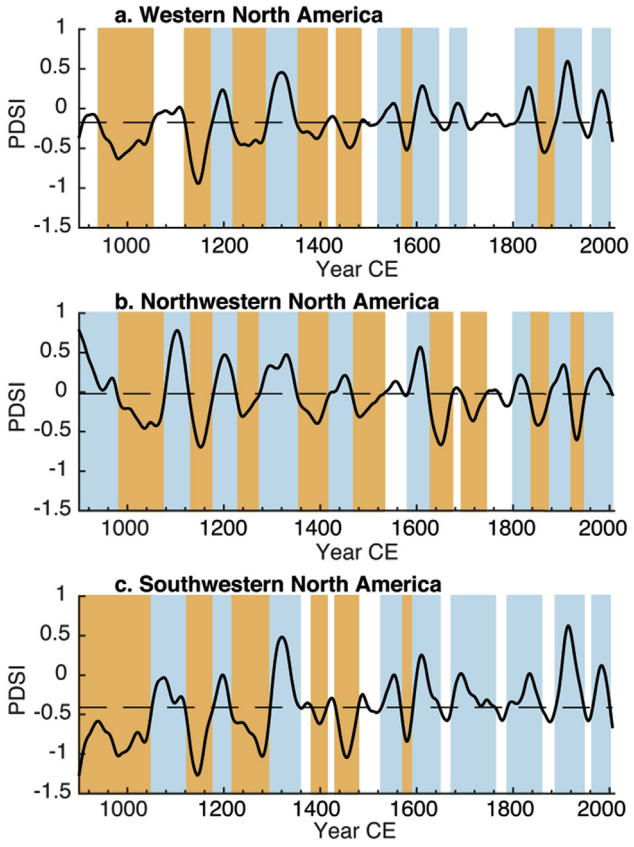

Fig. 3. Characterizing droughts and pluvials. Time series of averaged PDSI gridpoints for a) western North America, b) northwestern North America, and c) southwestern North America, spanning 900–2006 AD, and smoothed with a 50-yr cubic smoothing spline. Droughts and pluvials are shown in brown and blue respectively. (For interpretation of the references to colour in this figure legend, the reader is referred to the web version of this article.)

are more representative of the spatial pattern of interannual variability than of longer timescale phenomena. Fig. 5 shows histograms of teleconnection correlations with NADA during the wettest pluvial and driest drought years. The dry drought years have average teleconnection strengths of −0.39 (NINO3), −0.28 (PDO) and 0.15 (AMO). Wet pluvial years have a weaker teleconnection relationship than dry drought years, with correlations of 0.29 (NINO3), 0.21 (PDO), and −0.12 (AMO). Although the signs of the teleconnection pattern relationships are largely consistent with those of the modern period, the distribution of teleconnection pattern values indicates a range in the direction and strength of these relationships even during the extreme years (e.g., Kumar et al., 2013).

3.3. Spectral analysis

Spectral analysis shows WNA PDSI has significant spectral peaks around 143, 30, and 11 years, as well as between three and four years, during the MCA (Fig. 6a). In contrast, the post-MCA period shows greater spectral strength at periods of 4–8 years, with an additional lower peak at 22 years. (Fig. 6b). Spectral peaks in the teleconnection series do not correspond with these differences between MCA and post MCA PDSI. The NINO3 teleconnection series has a significant peak at 9.5 years as well as several at less than five years during the MCA (Fig. 6c). Post-MCA, the NINO3 has a significant peak at 5.2 years, with a number of other weakly significant peaks (Fig. 6d). During the MCA, the AMO teleconnection series has prominent significant spectral peaks at 33.4 years and 9.6 years, contrasting with a prominent 63.9-year post-MCA AMO spectral peak.

Table 2
Drought and pluvial intervals for WNA.

WNA drought intervals (CE)	WNA pluvial intervals (CE)
941–1052	1176–1215
1120–1175	1290–1350
1216–1289	1521–1565
1351–1413	1594–1644
1435–1483	1670–1702
1566–1593	1806–1848
1849–1888	1889–1940
	1966–2000

3.4. PaleoSST reconstruction anomaly maps

This analysis is beginning to push the limits of geochronological accuracy and resolution for SST reconstructions; nevertheless, general patterns of background SST patterns emerge in our analysis. The strongest signals for both the MCA/post-MCA and drought/pluvial composites occur in the northeast Atlantic and in the western tropical Pacific. SST anomalies were variable but generally cool during the MCA in the eastern tropical Pacific, warm in the western Pacific, and northern and eastern Atlantic, and variable in the western Atlantic (Fig. 7a). The post-MCA anomalies are a reversal of this pattern (Fig. 7b), which is expected because of how the anomalies were calculated. Both patterns are consistent with a La Niña-like MCA and an El Niño-like post MCA. Combined drought and pluvial periods for WNA also generally have La Niña-like and El Niño-like proxy SST anomalies in the Pacific respectively (Fig. 7c–d). The drought SST anomaly pattern in WNA (Fig. 7c) shows more broad scale warming in the North Atlantic, in contrast to the stronger warm anomalies focused in the northern and eastern Atlantic during the MCA (Fig. 7a). The WNA pluvial pattern shows generally warmer SSTs in the eastern tropical Pacific and Gulf of Mexico and cooler SSTs in the northern and eastern Atlantic and western Pacific (Fig. 7d).

4. Discussion

Teleconnection patterns reflected in the gridded PDSI and proxy SST reconstructions provide a way to examine the SST forcing mechanisms of past WNA climate variability. Below we assess evidence regarding each of the research questions set forth in the introduction.

4.1. Are differences in WNA hydroclimate between the MCA and post-MCA linked to SSTs?

The MCA has been characterized by widespread and persistent drought in WNA (e.g., Cook et al., 2004; Herweijer et al., 2007; Woodhouse and Overpeck, 1998). Here we confirm this characterization, identifying more long-lasting drought events in WNA during the MCA than in post-MCA years (Fig. 3), as well as an increase in low frequency variance of PDSI during the MCA (Fig. 6a). Were these differences in WNA climate forced by ocean/atmosphere circulation patterns related to SSTs?

Previous work has attributed the WNA MCA climate to the tropical Pacific (e.g., Conroy et al., 2009a; Graham et al., 2007; Herweijer et al., 2007; Seager et al., 2007). In this analysis, we show that strong tropical Pacific teleconnection patterns were present throughout the past millennium (Fig. 4a). Yet there was

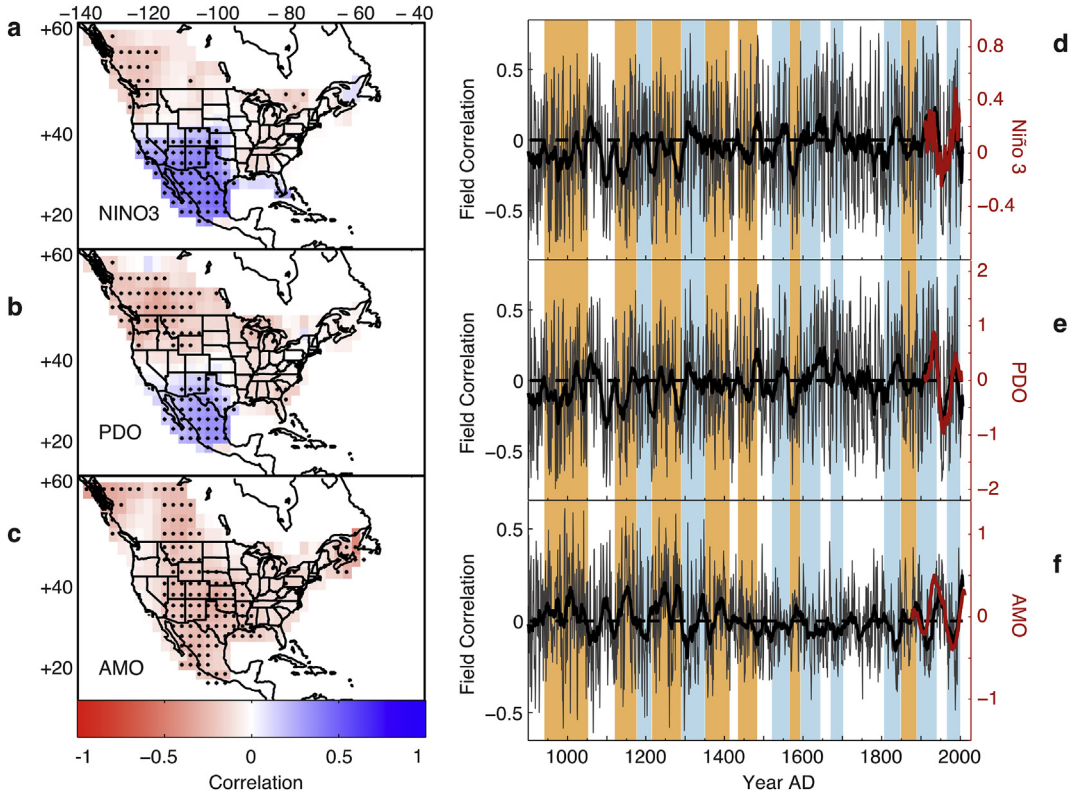

Fig. 4. Teleconnection pattern analysis. Maps (a–c) show the modern teleconnection relationship (correlation fields) between instrumental climate modes including NINO3, PDO, and the AMO and the last ~100 years of the NADA respectively. Negative correlations are in red and positive correlations are in blue. Black dots indicate local grid correlation significance ($p \leq 0.1$). The time series (d–f) show spatial correlation values between the maps (left) and annual tree-ring reconstructed PDSI patterns in the NADA over the past millennium. The heavy black lines are smoothed with a 20-year moving average. The instrumental climate modes smoothed with a 20-year moving average are plotted on the teleconnection strength time series in red. The vertical brown and blue bars reflect the drought and pluvial events in WNA respectively. (For interpretation of the references to colour in this figure legend, the reader is referred to the web version of this article.)

little change in the strength or direction of Pacific teleconnection patterns during the MCA compared to the post-MCA period. In addition, teleconnection patterns do not indicate that stronger or more frequent La Niña events forced MCA megadroughts. Because of the greater frequency of drought in WNA during the MCA, and the correspondence between dry years and La Niña-like conditions, and less drought, along with the relationship between wet years and El Niño-like conditions the reverse for wet years (Fig. 5a and b), this result was somewhat unexpected. Furthermore, spectral analysis of the NINO3 teleconnection series does not show an increase in low-frequency variance coincident with greater persistence in PDSI during the MCA (Fig. 6c).

Changes in Atlantic SSTs could be another mechanism forcing the MCA/post-MCA climate differences in WNA. Hidalgo (2004) suggest that much of the low frequency variance in past WNA hydroclimate variability is linked to North Atlantic SST variations related to the AMO. The AMO teleconnection series (Fig. 4f) has a weaker relationship with WNA climate than Pacific teleconnection series ($r = -0.43$ versus $r = 0.77$), but the overall AMO teleconnection strength is greater during the MCA. This could indicate the North Atlantic had a stronger influence on WNA climate during the MCA. In modern times the North Atlantic varies on long (60–80 year) timescales. It is possible that a stronger WNA-North Atlantic teleconnection during the MCA could have modulated the timing of droughts and pluvials, as well as the underlying low-frequency climate variability. Spectral analysis of the AMO teleconnection series, however, shows no MCA spectral peaks that correspond with the enhanced low frequency PDSI variability (Fig. 6a and e).

In contrast to the tree-ring based WNA teleconnection patterns, proxy SST records, particularly in the western tropical Pacific and eastern North Atlantic, indicate a shift from a warm North Atlantic and La Niña-like Pacific pattern during the MCA to a cool North Atlantic and El Niño-like Pacific pattern during the post-MCA (Fig. 7a–b). These results suggest a La Niña-like based state in SSTs in the MCA. As discussed above, WNA drought patterns show neither an increased strength nor frequency in La Niña teleconnection patterns during the MCA, which is inconsistent with persistent La Niña as a dominant driver for the MCA megadroughts. If La Niña conditions were responsible for the WNA MCA climate, the associated teleconnection may have imparted a different spatial footprint of drought. There is some agreement between North Atlantic teleconnection patterns and the SST proxy records, where warmer Atlantic background MCA SSTs (e.g., Oglesby et al., 2012) coincided with increased AMO teleconnection strength.

Prior research results using Pacific precipitation proxy records suggest a more complex La Niña-like MCA story (e.g., Yan et al., 2011). Precipitation reconstructions from the eastern and western tropical Pacific show increases in MCA eastern tropical Pacific runoff intensity (Fig. 8c; Conroy et al., 2008), and decreases in western tropical Pacific rainfall (Fig. 8d; Tierney et al., 2010), which is further supported by an increase in western tropical Pacific sea surface salinity (Fig. 8e, Oppo et al., 2009). These precipitation and salinity conditions are the opposite from what would be expected based on the SST proxy data for the MCA and post MCA periods, with the precipitation records suggesting an El Niño-like MCA and a La Niña-like post-MCA (e.g., Conroy et al., 2010; Oppo et al., 2009; Tierney et al., 2010; Yan et al., 2011). A likely explanation for this enigma may be stronger El Niño events embedded within largely

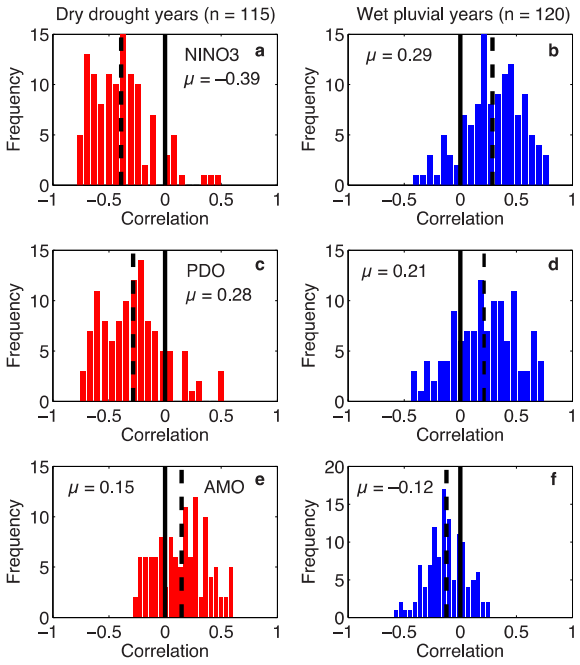

Fig. 5. Teleconnection strength during the driest WNA drought years and the wettest WNA pluvial years. Dry drought years are defined as years with PDSI < −1 during droughts and wet pluvial years as PDSI >1 during pluvials. Histograms show the frequency of positive and negative teleconnection patterns during these extreme years. Negative ENSO correlations indicate a La Niña type teleconnection pattern. Positive AMO correlations indicate a warm North Atlantic type teleconnection pattern. The solid vertical lines show correlations of zero and the dashed vertical lines show the mean correlation strengths.

persistent periods of La Niña-like tropical Pacific conditions (e.g., Conroy et al., 2009b; Routson et al., 2011). Yet a record of ENSO variability using $\delta^{18}O$ from single-shell *G. ruber* in the eastern tropical Pacific indicates less ENSO variance during the MCA (Rustic et al., 2015). Finally, a recent multiproxy ENSO reconstruction shows no clear shift in the background state of the tropical Pacific between the MCA and post-MCA (Emile-Geay et al., 2013). The widely varying evidence suggests that conditions in the tropical Pacific during the MCA may have been complex, with no modern analogue (e.g., Tierney et al., 2010). Nonetheless, proxy observations of SSTs strongly suggest background SSTs during the MCA were La Niña-like followed by El Niño-like post-MCA conditions.

Some of the discrepancies between the teleconnection and SST proxy data results may be due to the tree-ring based PDSI teleconnection patterns better reflecting annual to multidecadal variability and the SST proxy data better reflecting century-scale variability. The broad spatial and temporal scale differences between the MCA and post-MCA are more likely to be highlighted by the SST data whereas the variability of PDSI teleconnections within the MCA and post-MCA periods are more strongly represented in the tree-ring data.

4.2. *What evidence links WNA megadroughts and megapluvials to SST forcing during the past millennium?*

Although the teleconnection patterns do not reflect marked differences between MCA and post MCA period, they do help elucidate the forcing mechanisms associated with individual drought and pluvial events. For example, the late 16th century megadrought stands out, characterized by a correspondence between dry conditions and La Niña patterns between 1566 and 1578, along with a positive AMO. This is in support of the La Niña-forcing mechanism hypothesis for this drought set forth by Stahle et al.

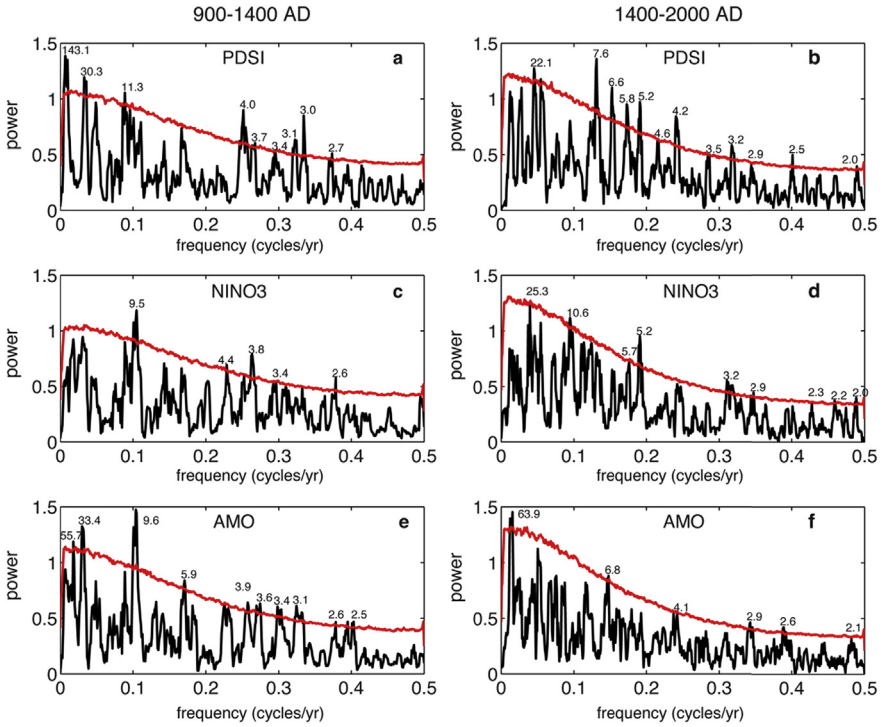

Fig. 6. Spectral analysis. Power spectra of WNA PDSI (a–b), NINO3 teleconnection series (c–d), and the AMO teleconnection series (e–f) during the MCA (900–1400 AD, left panels) and post-MCA (1400–2007 AD, right panels) periods. Peaks significant above the 95% red noise confidence interval (red) are denoted in years. (For interpretation of the references to colour in this figure legend, the reader is referred to the web version of this article.)

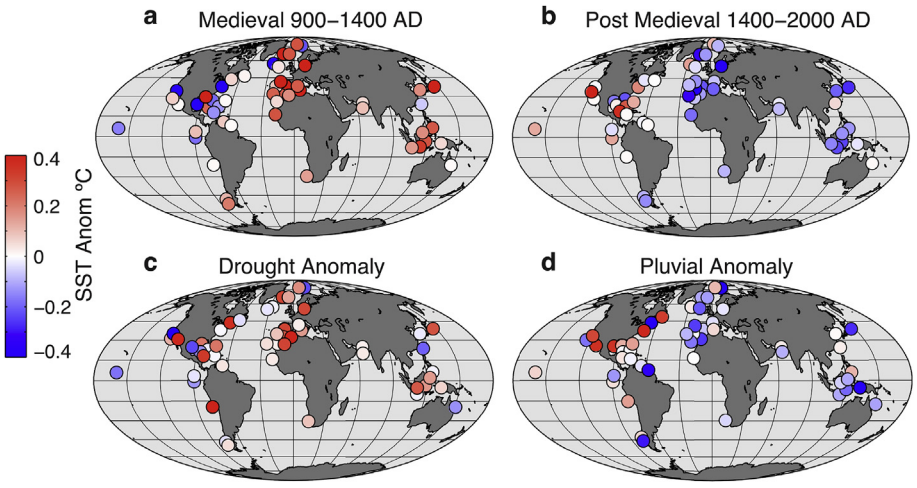

Fig. 7. Proxy SST anomaly maps. SST anomalies during (a) the medieval period, (b) the post medieval period. Panels (c–d) show SST anomalies during persistent drought and pluvial events in WNA. Drought and pluvial events are defined by the smoothed series in Fig. 3. Proxy SST anomalies are computed with respect to the 900–2000 AD mean, or the series length mean if shorter than the analysis period.

(2000). Many of the MCA droughts also have sequences of La Niña-like PDSI patterns, but they tend to not persist through the entire events (e.g., the first half of the 1125–1175 drought and the last part of the drought ending in the late 1300s). In a similar way, AMO teleconnections tend to be positive (warm Atlantic SSTs) but variable over the periods of MCA drought. The teleconnection patterns during pluvials were generally weaker than for droughts. Pluvials during the 17th and 18th centuries had sequences of El Niño-like patterns, but the MCA pluvials show a weaker correspondence to El Niño teleconnections. Teleconnection pattern relationships with AMO during pluvials tend to be negative (cool Atlantic) during at least parts of the pluvial periods in both the MCA and post-MCA periods. These variable relationships become stronger when the most extreme wet and dry years are examined (Fig. 5).

In examining the relationship between WNA megadroughts and pluvials to SST forcing, the resolution and age control of proxy SST reconstructions, which are much lower than that of the tree-ring based teleconnection patterns, must be considered. Caution is advised when interpreting these records on relatively short drought and pluvial-length, decadal timescales. To help address the resolution limitations of the proxy SST data, we treated the drought and pluvial as (separate) composites. These averages however, tend to reflect the broad periods when most of the drought and pluvial events occurred. Nonetheless, there are important differences between drought and pluvial periods. Overall, the SST reconstructions suggest that droughts and pluvials in WNA tend to have La Niña-like and El Niño-like background conditions, respectively (Fig. 7c–d). Proxy SST anomalies in the North Atlantic warm during WNA droughts (Fig. 7c). This contrasts with the overall MCA, which has stronger warming in the North and Eastern Atlantic and variable SSTs in the Western Atlantic. Pluvials in WNA are associated with cooling especially in the North and Eastern Atlantic, but warming in the Gulf of Mexico (Fig. 7d).

4.3. Do SST/pluvial associations vary with multidecadal variability, for example, within the MCA?

Our third research question addresses the two pluvials that occurred in WNA during the MCA between 1176-1215 and 1290–1350 respectively. How could MCA pluvials occur during a time where SST proxy records show persistent La Niña conditions in the Pacific? This could partially be due to the low temporal resolution of the SST proxy data, but these pluvials may also be a manifestation of the complexities in the tropical Pacific SST and precipitation proxies we assessed. The two pluvials are pronounced in the WNA PDSI average, and are widespread across the region (Fig. 3).

Composite maps of PDSI averaged across the years of the two pluvials show they have relatively different spatial patterns across North America (Fig. 9). The earlier pluvial is characterized by a strong east-west dipole, where WNA is wet and eastern North America is dry. The smoothed NINO3 teleconnection series is neutral during this early pluvial and the smoothed AMO teleconnection series is only slightly negative (Fig. 10). The east-west dipole pattern of the 1176–1215 pluvial (Fig. 9) is strikingly reminiscent of the second mode of North American drought variability identified by Woodhouse et al. (2009). Their first mode defined by the first principal component (PC1) of the NADA reflects an ENSO type north-south dipole pattern, and their second mode (PC2) reflects an east-west dipole they link to the position and sinuosity of the polar jet stream and the Northern Hemispheric annular mode (NAM). During the early 1176–1215 pluvial, PC2 has a positive anomaly, linking the potential cause of this event to the NAM, characterized by variations in patterns of atmospheric pressure (Fig. 10).

The later pluvial (1290–1350) had a widespread pattern, spanning much of the continent, with the largest anomalies centered directly in the middle of WNA (Fig. 9). The widespread pattern of the second MCA pluvial is reminiscent of the AMO teleconnection pattern. The unsmoothed AMO teleconnection time series has a sequence of negative years from 1296 AD, through 1305 AD. The smoothed series in Fig. 10 also shows the AMO was negative during the earlier portion of this pluvial, suggesting that the AMO may have played a role in causing the second MCA pluvial. The drought modes (Woodhouse et al., 2009) are less clear during the second MCA pluvial, showing anomalies in both PC1 and PC2. Together the evidence suggests MCA pluvials were forced by a combination of factors, which likely included the NAM during the first pluvial and perhaps North Atlantic SST variability during the second pluvial. In both cases the pluvials are consistent with known mechanisms *and* the presence of La Niña-like conditions in the tropical Pacific. Notably, neither pluvial map has a characteristic ENSO dipole pattern when averaged across the entire pluvial duration (Fig. 9), which was also true during the early 20th century pluvial (Woodhouse et al., 2005).

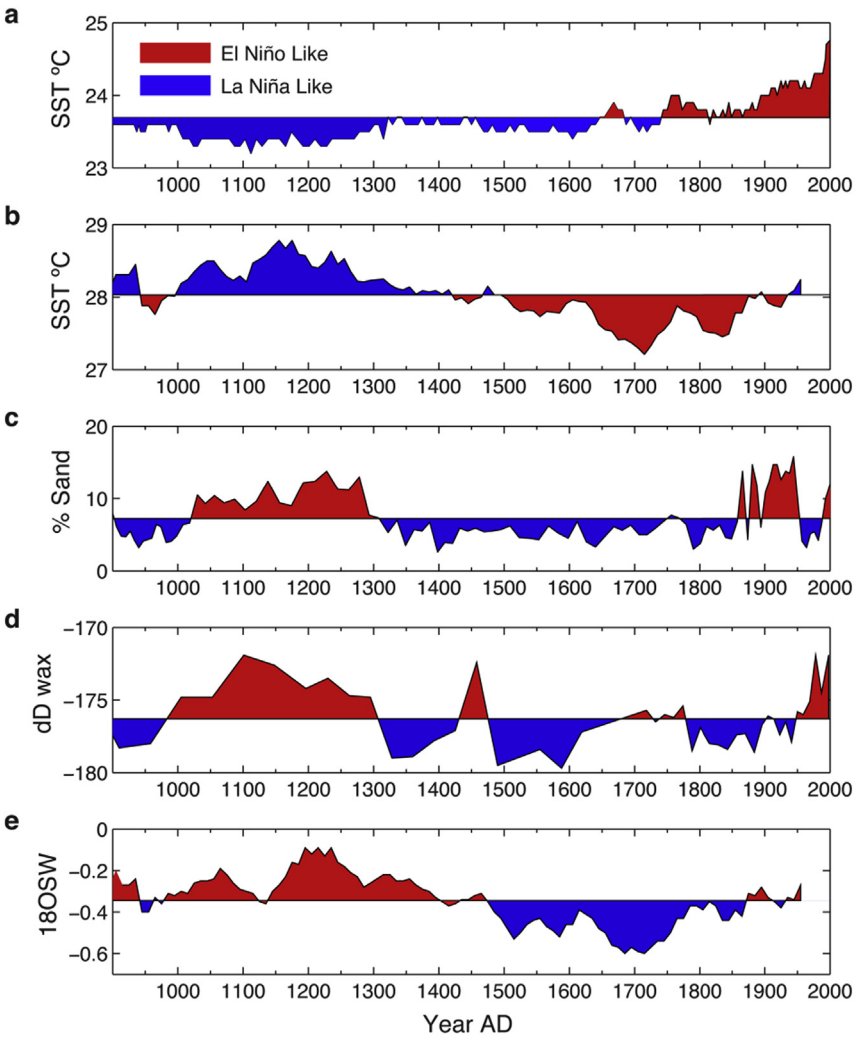

Fig. 8. Tropical Pacific SST and precipitation ENSO reconstructions in apparent contradiction. Records are from both sides of the tropical Pacific basin. Red coloring indicates El Niño like conditions and blue colour indicates La Niña like conditions. a) Diatom inferred SST from the Lake El Junco in the Galapagos Islands (Conroy et al., 2009b), b) Mg/Ca inferred SST from the Indo Pacific Warm Pool (Oppo et al., 2009), c) grain size inferred precipitation intensity from Lake El Junco (Conroy et al., 2008), d) deuterium leaf wax isotope precipitation reconstruction from the Indo Pacific Warm Pool (Tierney et al., 2010), and e) $\delta^{18}O$ of sea water inferred salinity reconstruction from the Indo Pacific Warm Pool (Oppo et al., 2009). (For interpretation of the references to colour in this figure legend, the reader is referred to the web version of this article.)

5. Conclusion

Reassessing the evidence linking SSTs to climate over the past millennium reveals both complexities and insights into the forcing mechanisms of WNA hydroclimate variability. Consistent with previous research (e.g., Conroy et al., 2009a; Feng et al., 2008, 2010; Graham et al., 2007; Herweijer et al., 2007; Oglesby et al., 2012; Seager et al., 2007), our analysis shows centennial-scale shifts in

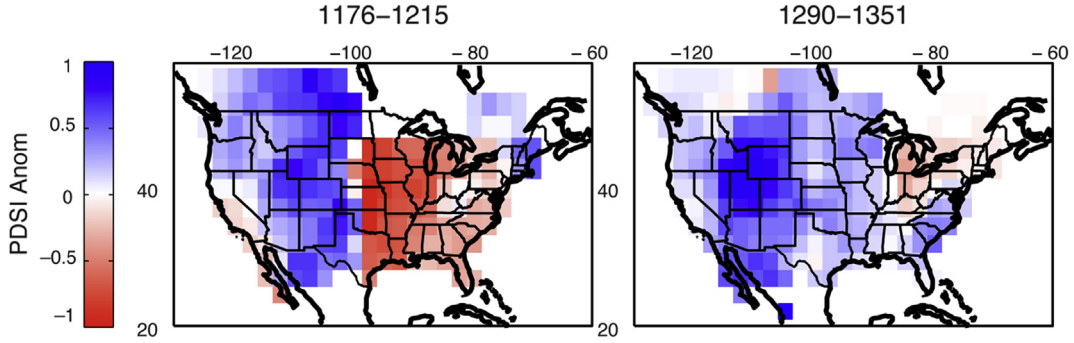

Fig. 9. Medieval pluvials. Reconstructed PDSI maps for MCA pluvials including the 1176–1215 AD and 1290–1351 AD events. Anomalies are computed with respect to the 900–2007 AD mean.

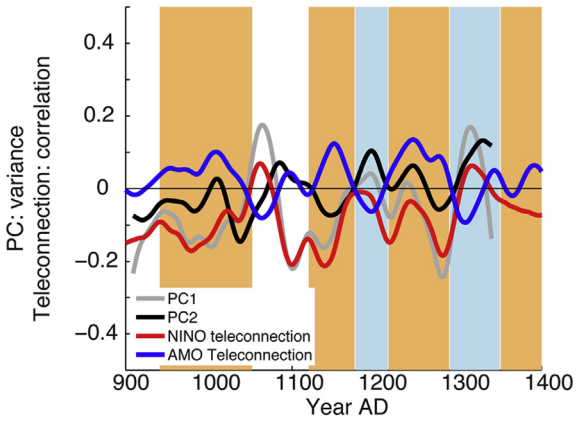

Fig. 10. Potential drivers of MCA pluvials. The MCA pluvial intervals are delineated by the vertical blue bars. The leading principal components of WNA PDSI from Woodhouse et al., 2009 are shown in grey (PC1) and black (PC2). NINO3 and AMO teleconnection strength time series are shown in red and blue respectively (this study). All series are smoothed with a 50-year cubic smoothing spline. The units for the PCs are in variance and the units for the teleconnection time series are in r-value correlation and plotted on the same axis. The first pluvial shows a positive, albeit weak, PC2 anomaly and a similarly weak negative AMO anomaly. The second pluvial shows a combination of potential forcing mechanisms, including El Niño-like and negative AMO-like teleconnection patterns, positive, or El Niño-like PC1, and a positive NAM type PC2. (For interpretation of the references to colour in this figure legend, the reader is referred to the web version of this article.)

drought/pluvial frequency and persistence observed between the MCA and post-MCA were accompanied by SST background changes from a La Niña-like Pacific and warm North Atlantic to an El Niño-like Pacific and cold North Atlantic. The large compilation of SST reconstructions presented here show the eastern North Atlantic and western tropical Pacific have the most agreement and strongest signal among the SST proxy records. Additional evidence, such as precipitation reconstructions, suggest MCA/post-MCA conditions in the tropical Pacific were complex, and likely more nuanced than suggested by the background SSTs alone. Furthermore, teleconnection patterns preserved in WNA tree-ring reconstructed PDSI maps show little evidence that La Niña teleconnections were more frequent during the MCA, but the strength of AMO teleconnections increased somewhat. If more persistent or frequent La Niña conditions forced WNA MCA climate, the teleconnection fingerprint may have been different. The difference in results for the SST proxy data and the tree-ring based teleconnection patterns may also be due in part to the different scales of spatial and temporal variability captured by these different types of climate proxy records.

Teleconnection patterns suggest both the Pacific and Atlantic likely played a role in forcing persistent WNA droughts and pluvials over the past millennium. The driest years within droughts and the wettest years within pluvials had stronger teleconnection patterns than the events as a whole. Iconic droughts like the 16th century megadrought and some medieval droughts had sequences of La Niña teleconnection patterns, implicating the tropical Pacific as a causal mechanism. More wide-spread events, characteristic during the MCA, have stronger correlations to the AMO teleconnection pattern. Reconstructed SST patterns indicate La Niña-like conditions in the Pacific and warm North Atlantic SSTs accompanied droughts, while El Niño-like conditions and cool North Atlantic SSTs accompanied pluvials. These patterns in-part reflect the broader MCA/post-MCA SST patterns during which most of the droughts and pluvials occurred respectively.

Finally, two MCA pluvials appear to have been forced by separate mechanisms. The earlier pluvial had a spatial pattern associated with the NAM, while the widespread pattern of the later pluvial has a stronger relationship with the North Atlantic teleconnection pattern. Neither of these hypothesized mechanisms are inconsistent with a La-Niña like Pacific, underscoring that SST background conditions alone cannot explain WNA hydroclimate.

Acknowledgements

We thank the National Oceanic and Atmospheric Administration (NOAA, NA11OAR4310162), the National Science Foundation (AGS1243125), the Science Foundation Arizona Bisgrove Scholars Fellowship program (BSP 0544-13), the NOAA funded Climate Assessment for the Southwest, the University of Arizona Department of Geoscience, and the Northern Arizona University School of Earth Science and Environmental Sustainability for contributing funding and support for this research. We also thank reviewers Dr. Gregory McCabe and two anonymous reviewers for their time, insights, and feedback.

Appendix A. Supplementary data

Supplementary data related to this article can be found at http://dx.doi.org/10.1016/j.quascirev.2016.06.017.

References

Abrantes, F., Lebreiro, S., Rodrigues, T., Gil, I., Bartels-Jónsdóttir, H., Oliveira, P., Kissel, C., Grimalt, J.O., 2005. Shallow-marine sediment cores record climate variability and earthquake activity off Lisbon (Portugal) for the last 2000 years. Quat. Sci. Rev. 24, 2477–2494. http://dx.doi.org/10.1016/j.quascirev.2004.04.009.

Batehup, R., McGregor, S., Gallant, A., 2015. The influence of non-stationary ENSO teleconnections on reconstructions of paleoclimate using a pseudoproxy framework. Clim. Past Discuss. 11, 3853–3895. http://dx.doi.org/10.5194/cpd-11-3853-2015.

Black, D.E., Abahazi, M.A., Thunell, R.C., Kaplan, A., Tappa, E.J., Peterson, L.C., 2007. An 8-century tropical Atlantic SST record from the Cariaco Basin: Baseline variability, twentieth-century warming, and Atlantic hurricane frequency. Paleoceanography 22, PA4204. http://dx.doi.org/10.1029/2007PA001427.

Bonnet, S., de Vernal, A., Hillaire-Marcel, C., Radi, T., Husum, K., 2010. Variability of sea-surface temperature and sea-ice cover in the Fram Strait over the last two millennia. Mar. Micropaleontol. 74, 59–74. http://dx.doi.org/10.1016/j.marmicro.2009.12.001.

Burgman, R., Seager, R., Clement, A., Herweijer, C., 2010. Role of tropical Pacific SSTs in global medieval hydroclimate: a modeling study. Geophys. Res. Lett. 37, L06705. http://dx.doi.org/10.1029/2009GL042239.

Cayan, D.R., Redmond, K.T., Riddle, L.G., 1999. ENSO and hydrologic extremes in the western United States. J. Clim. 12, 2881–2893. http://dx.doi.org/10.1175/1520-0442(1999)012<2881:EAHEIT>2.0.CO;2.

Cobb, K.M., Charles, C.D., Cheng, H., Edwards, R.L., 2003. El Niño/Southern Oscillation and tropical Pacific climate during the last millennium. Nature 424, 271–276. http://dx.doi.org/10.1038/nature01779.

Cole, J.E., Cook, E.R., 1998. The changing relationship between ENSO variability and moisture balance in the continental United States. Geophys. Res. Lett. 25, 4529–4532. http://dx.doi.org/10.1029/1998GL900145.

Conroy, J.L., Overpeck, J.T., Cole, J.E., Shanahan, T.M., Steinitz-Kannan, M., 2008. Holocene changes in eastern tropical Pacific climate inferred from a Galápagos lake sediment record. Quat. Sci. Rev. 27, 1166–1180. http://dx.doi.org/10.1016/j.quascirev.2008.02.015.

Conroy, J.L., Overpeck, J.T., Cole, J.E., Steinitz-Kannan, M., 2009a. Variable oceanic influences on western North American drought over the last 1200 years. Geophys. Res. Lett. 36, L17703. http://dx.doi.org/10.1029/2009GL039558.

Conroy, J.L., Restrepo, A., Overpeck, J.T., Steinitz-Kannan, M., Cole, J.E., Bush, M.B., Colinvaux, P.A., 2009b. Unprecedented recent warming of surface temperatures in the eastern tropical Pacific Ocean. Nat. Geosci. 2, 46–50. http://dx.doi.org/10.1038/ngeo390.

Conroy, J.L., Overpeck, J.T., Cole, J.E., 2010. El Niño/Southern Oscillation and Changes in the Zonal Gradient of Tropical Pacific Sea Surface Temperature over the Last 1.2 Ka, p. 18.

Cook, E.R., Krusic, P.J., 2008. North American Summer PDSI Reconstructions. version 2a. In: IGBP PAGES/World Data Center for Paleoclimatology Data Contribution Series, 46.

Cook, E.R., Briffa, K.R., Meko, D.M., Graybill, D.A., Funkhouser, G., 1995. The "segment length curse" in long tree-ring chronology development for palaeoclimatic studies. Holocene 5, 229–237. http://dx.doi.org/10.1177/095968369500500211.

Cook, E.R., Woodhouse, C.A., Eakin, C.M., Meko, D.M., Stahle, D.W., 2004. Long-term

aridity changes in the western United States. Science 306, 1015–1018. http://dx.doi.org/10.1126/science.1102586.
Cook, E.R., Seager, R., Cane, M.A., Stahle, D.W., 2007. North American drought: reconstructions, causes, and consequences. Earth Sci. Rev. 81, 93–134. http://dx.doi.org/10.1016/j.earscirev.2006.12.002.
Cook, B.I., Cook, E.R., Anchukaitis, K.J., Seager, R., Miller, R.L., 2010a. Forced and unforced variability of twentieth century North American droughts and pluvials. Clim. Dyn. 37, 1097–1110. http://dx.doi.org/10.1007/s00382-010-0897-9.
Cook, E.R., Seager, R., Heim, R.R., Vose, R.S., Herweijer, C., Woodhouse, C., 2010b. Megadroughts in North America: placing IPCC projections of hydroclimatic change in a long-term palaeoclimate context. J. Quat. Sci. 25, 48–61. http://dx.doi.org/10.1002/jqs.1303.
Cook, B.I., Smerdon, J.E., Seager, R., Cook, E.R., 2014. Pan-continental droughts in North America over the last millennium. J. Clim. 27, 383–397. http://dx.doi.org/10.1175/JCLI-D-13-00100.1.
Cronin, T.M., Dwyer, G.S., Kamiya, T., Schwede, S., Willard, D.A., 2003. Medieval warm period, little ice age and 20th century temperature variability from Chesapeake Bay. Glob. Planet. Change 36, 17–29. http://dx.doi.org/10.1016/S0921-8181(02)00161-3.
Doose-Rolinski, H., Rogalla, U., Scheeder, G., Lückge, A., von Rad, U., 2001. High-resolution temperature and evaporation changes during the late Holocene in the northeastern Arabian sea. Paleoceanography 16, 358–367. http://dx.doi.org/10.1029/2000PA000511.
Eiríksson, J., Bartels-Jónsdóttir, H.B., Cage, A.G., Gudmundsdóttir, E.R., Klitgaard-Kristensen, D., Marret, F., Rodrigues, T., Abrantes, F., Austin, W.E.N., Jiang, H., Knudsen, K.-L., Sejrup, H.-P., 2006. Variability of the North Atlantic Current during the last 2000 years based on shelf bottom water and sea surface temperatures along an open ocean/shallow marine transect in western Europe. Holocene 16, 1017–1029. http://dx.doi.org/10.1177/0959683606hl991rp.
Emile-Geay, J., Cobb, K.M., Mann, M.E., Wittenberg, A.T., 2013. Estimating central equatorial Pacific SST variability over the past millennium. Part II: reconstructions and implications. J. Clim. 26, 2329–2352. http://dx.doi.org/10.1175/JCLI-D-11-00511.1.
Feng, S., Oglesby, R.J., Rowe, C.M., Loope, D.B., Hu, Q., 2008. Atlantic and Pacific SST influences on medieval drought in north America simulated by the community atmospheric model. J. Geophys. Res. 113, D11101. http://dx.doi.org/10.1029/2007JD009347.
Feng, S., Hu, Q., Oglesby, R.J., 2010. Influence of Atlantic sea surface temperatures on persistent drought in North America. Clim. Dyn. 37, 569–586. http://dx.doi.org/10.1007/s00382-010-0835-x.
Goni, M.A., Thunell, R.C., Woodwort, M.P., Müller-Karger, F.E., 2006. Changes in wind-driven upwelling during the last three centuries: Interocean teleconnections. Geophys. Res. Lett. 33, L15604. http://dx.doi.org/10.1029/2006GL026415.
Graham, N.E., Hughes, M.K., Ammann, C.M., Cobb, K.M., Hoerling, M.P., Kennett, D.J., Kennett, J.P., Rein, B., Stott, L., Wigand, P.E., Xu, T., 2007. Tropical Pacific – mid-latitude teleconnections in medieval times. Clim. Change 83, 241–285. http://dx.doi.org/10.1007/s10584-007-9239-2.
Gray, S.T., Graumlich, L.J., Betancourt, J.L., Pederson, G.T., 2004. A tree-ring based reconstruction of the Atlantic Multidecadal Oscillation since 1567 A.D. Geophys. Res. Lett. 31, L12205. http://dx.doi.org/10.1029/2004GL019932.
Gutiérrez, D., Bouloubassi, I., Sifeddine, A., Purca, S., Goubanova, K., Graco, M., Field, D., Méjanelle, L., Velazco, F., Lorre, A., Salvatteci, R., Quispe, D., Vargas, G., Dewitte, B., Ortlieb, L., 2011. Coastal cooling and increased productivity in the main upwelling zone off Peru since the mid-twentieth century. Geophys. Res. Lett. 38, L07603. http://dx.doi.org/10.1029/2010GL046324.
Hendy, E.J., Gagan, M.K., Alibert, C.A., McCulloch, M.T., Lough, J.M., Isdale, P.J., 2002. Abrupt decrease in tropical Pacific sea surface salinity at end of Little Ice Age. Science 295, 1511–1514. http://dx.doi.org/10.1126/science.1067693.
Hendy, I.L., Dunn, L., Schimmelmann, A., Pak, D.K., 2013. Resolving varve and radiocarbon chronology differences during the last 2000 years in the Santa Barbara Basin sedimentary record, California. Quat. Int. 310, 155–168. http://dx.doi.org/10.1016/j.quaint.2012.09.006. PACLIM: Proceedings of the 25th Pacific Climate Workshop, 2011.
Herweijer, C., Seager, R., Cook, E.R., Emile-Geay, J., 2007. North American droughts of the last millennium from a gridded network of tree-ring data. J. Clim. 20, 1353–1376. http://dx.doi.org/10.1175/JCLI4042.1.
Hidalgo, H.G., 2004. Climate precursors of multidecadal drought variability in the western United States. Water Resour. Res. 40, W12504. http://dx.doi.org/10.1029/2004WR003350.
Hu, Q., Feng, S., 2001. Variations of teleconnection of ENSO and interannual variation in summer rainfall in the Central United States. J. Clim. 14, 2469–2480. http://dx.doi.org/10.1175/1520-0442(2001)014<2469:VOTOEA>2.0.CO;2.
Hu, Q., Feng, S., 2012. AMO- and ENSO-driven summertime circulation and precipitation variations in north America. J. Clim. 25, 6477–6495. http://dx.doi.org/10.1175/JCLI-D-11-00520.1.
Isono, D., Yamamoto, M., Irino, T., Oba, T., Murayama, M., Nakamura, T., Kawahata, H., 2009. The 1500-year climate oscillation in the midlatitude North Pacific during the Holocene. Geology 37, 591–594. http://dx.doi.org/10.1130/G25667A.1.
Kam, J., Sheffield, J., Wood, E.F., 2014. Changes in drought risk over the contiguous United States (1901–2012): the influence of the Pacific and Atlantic Oceans. Geophys. Res. Lett. 41 http://dx.doi.org/10.1002/2014GL060973, 2014GL060973.
Kaplan, A., Cane, M.A., Kushnir, Y., Clement, A.C., Blumenthal, M.B., Rajagopalan, B., 1998. Analyses of global sea surface temperature 1856–1991. J. Geophys. Res. 103, 18. http://dx.doi.org/10.1029/97JC01736.
Keigwin, L.D., Sachs, J.P., Rosenthal, Y., 2003. A 1600-year history of the Labrador current off Nova scotia. Clim. Dyn. 21, 53–62. http://dx.doi.org/10.1007/s00382-003-0316-6.
Kennett, D.J., Kennett, J.P., 2000. Competitive and cooperative responses to climatic instability in coastal southern California. Am. Antiq. 65, 379–395. http://dx.doi.org/10.2307/2694065.
Kim, J.-H., Rimbu, N., Lorenz, S.J., Lohmann, G., Nam, S.-I., Schouten, S., Rühlemann, C., Schneider, R.R., 2004. North Pacific and north Atlantic sea-surface temperature variability during the Holocene. Quaternary science reviews. Holocene Clim. Var.– A Mar. Perspect. 23, 2141–2154. http://dx.doi.org/10.1016/j.quascirev.2004.08.010.
Kuhnert, H., Mulitza, S., 2011. Multidecadal variability and late medieval cooling of near-coastal sea surface temperatures in the eastern tropical North Atlantic. Paleoceanography 26, PA4224. http://dx.doi.org/10.1029/2011PA002130.
Kumar, A., Chen, M., Hoerling, M., Eischeid, J., 2013. Do extreme climate events require extreme forcings? Geophys. Res. Lett. 40, 3440–3445. http://dx.doi.org/10.1002/grl.50657.
Leduc, G., Schneider, R., Kim, J.-H., Lohmann, G., 2010a. Holocene and Eemian sea surface temperature trends as revealed by alkenone and Mg/Ca paleothermometry. Quat. Sci. Rev. 29, 989–1004. http://dx.doi.org/10.1016/j.quascirev.2010.01.004.
Leduc, G., Herbert, C.T., Blanz, T., Martinez, P., Schneider, R., 2010b. Contrasting evolution of sea surface temperature in the Benguela upwelling system under natural and anthropogenic climate forcings. Geophys. Res. Lett. 37, L20705. http://dx.doi.org/10.1029/2010GL044353.
Linsley, B.K., Rosenthal, Y., Oppo, D.W., 2010. Holocene evolution of the Indonesian throughflow and the western Pacific warm pool. Nat. Geosci. 3, 578–583. http://dx.doi.org/10.1038/ngeo920.
Lund, D.C., Curry, W., 2006. Florida Current surface temperature and salinity variability during the last millennium. Paleoceanography 21, PA2009. http://dx.doi.org/10.1029/2005PA001218.
Mantua, N.J., Hare, S.R., Zhang, Y., Wallace, J.M., Francis, R.C., 1997. A pacific interdecadal climate oscillation with impacts on salmon production. Bull. Am. Meteor. Soc. 78, 1069–1079. http://dx.doi.org/10.1175/1520-0477(1997)078<1069:APICOW>2.0.CO;2.
McCabe, G.J., Dettinger, M.D., 1999. Decadal variations in the strength of ENSO teleconnections with precipitation in the western United States. Int. J. Climatol. 19, 1399–1410. http://dx.doi.org/10.1002/(SICI)1097-0088(19991115)19:13<1399::AID-JOC457>3.0.CO;2-A.
McCabe, G.J., Wolock, D.M., 2013. Variability common to global sea surface temperatures and runoff in the conterminous United States. J. Hydrometeor 15, 714–725. http://dx.doi.org/10.1175/JHM-D-13-097.1.
McCabe, G.J., Palecki, M.A., Betancourt, J.L., 2004. Pacific and Atlantic Ocean influences on multidecadal drought frequency in the United States. PNAS 101, 4136–4141. http://dx.doi.org/10.1073/pnas.0306738101.
McCabe, G.J., Betancourt, J.L., Gray, S.T., Palecki, M.A., Hidalgo, H.G., 2008. Associations of multi-decadal sea-surface temperature variability with US drought. Quat. Int. 188, 31–40. http://dx.doi.org/10.1016/j.quaint.2007.07.001. The 22nd Pacific Climate Workshop.
McGregor, H.V., Dima, M., Fischer, H.W., Mulitza, S., 2007. Rapid 20th-Century Increase in coastal upwelling off northwest Africa. Science 315, 637–639. http://dx.doi.org/10.1126/science.1134839.
Meko, D.M., Woodhouse, C.A., Baisan, C.A., Knight, T., Lukas, J.J., Hughes, M.K., Salzer, M.W., 2007. Medieval drought in the upper Colorado River Basin. Geophys. Res. Lett. 34.
Miettinen, A., Divine, D., Koç, N., Godtliebsen, F., Hall, I.R., 2012. Multicentennial variability of the sea surface temperature gradient across the subpolar North Atlantic over the last 2.8 kyr. J. Clim. 25, 4205–4219. http://dx.doi.org/10.1175/JCLI-D-11-00581.1.
Mohtadi, M., Romero, O.E., Kaiser, J., Hebbeln, D., 2007. Cooling of the southern high latitudes during the Medieval Period and its effect on ENSO. Quat. Sci. Rev. 26, 1055–1066. http://dx.doi.org/10.1016/j.quascirev.2006.12.008.
Moreno, A., Pérez, A., Frigola, J., Nieto-Moreno, V., Rodrigo-Gámiz, M., Martrat, B., González-Sampériz, P., Morellón, M., Martín-Puertas, C., Corella, J.P., Belmonte, Á., Sancho, C., Cacho, I., Herrera, G., Canals, M., Grimalt, J.O., Jiménez-Espejo, F., Martínez-Ruiz, F., Vegas-Vilarrúbia, T., Valero-Garcés, B.L., 2012. The medieval climate anomaly in the Iberian Peninsula reconstructed from marine and lake records. Quat. Sci. Rev. 43, 16–32. http://dx.doi.org/10.1016/j.quascirev.2012.04.007.
Newman, M., Compo, G.P., Alexander, M.A., 2003. ENSO-forced variability of the Pacific decadal oscillation. J. Clim. 16, 3853–3857. http://dx.doi.org/10.1175/1520-0442(2003)016<3853:EVOTPD>2.0.CO;2.
Newton, A., Thunell, R., Stott, L., 2006. Climate and hydrographic variability in the Indo-Pacific Warm Pool during the last millennium. Geophys. Res. Lett. 33, L19710. http://dx.doi.org/10.1029/2006GL027234.
Newton, A., Thunell, R., Stott, L., 2011. Changes in the Indonesian throughflow during the past 2000 yr. Geology 39, 63–66. http://dx.doi.org/10.1130/G31421.1.
Nieto-Moreno, V., Martínez-Ruiz, F., Willmott, V., García-Orellana, J., Masqué, P., Sinninghe Damsté, J.S., 2013. Climate conditions in the westernmost Mediterranean over the last two millennia: an integrated biomarker approach. Org. Geochem. 55, 1–10. http://dx.doi.org/10.1016/j.orggeochem.2012.11.001.
Nowak, K., Hoerling, M., Rajagopalan, B., Zagona, E., 2012. Colorado River Basin hydroclimatic variability. J. Clim. 25, 4389–4403. http://dx.doi.org/10.1175/JCLI-D-11-00406.1.

Oglesby, R., Feng, S., Hu, Q., Rowe, C., 2012. The role of the Atlantic Multidecadal Oscillation on medieval drought in North America: synthesizing results from proxy data and climate models. Global and Planetary Change 84–85, 56–65. http://dx.doi.org/10.1016/j.gloplacha.2011.07.005. Perspectives on Climate in Medieval Time.

Oppo, D.W., Rosenthal, Y., Linsley, B.K., 2009. 2,000-year-long temperature and hydrology reconstructions from the Indo-Pacific warm pool. Nature 460, 1113–1116. http://dx.doi.org/10.1038/nature08233.

Palmer, W.C., 1965. Meteroological Drought. Research Paper. U.S. Weather Bureau, Office of Climatology, Washington D.C.

Redmond, K.T., Koch, R.W., 1991. Surface climate and streamflow variability in the Western United States and their relationship to large-scale circulation indices. Water Resour. Res. 27, 2381–2399. http://dx.doi.org/10.1029/91WR00690.

Reynolds, R.W., Rayner, N.A., Smith, T.M., Stokes, D.C., Wang, W., 2002. An improved in situ and satellite SST analysis for climate. J. Clim. 15, 1609–1625. http://dx.doi.org/10.1175/1520-0442(2002)015<1609:AIISAS>2.0.CO;2.

Richey, J.N., Poore, R.Z., Flower, B.P., Quinn, T.M., 2007. 1400 yr multiproxy record of climate variability from the northern Gulf of Mexico. Geology 35, 423–426. http://dx.doi.org/10.1130/G23507A.1.

Richey, J.N., Poore, R.Z., Flower, B.P., Quinn, T.M., Hollander, D.J., 2009. Regionally coherent little ice age cooling in the Atlantic warm pool. Geophys. Res. Lett. 36 http://dx.doi.org/10.1029/2009GL040445. L21703.

Richter, T.O., Peeters, F.J.C., van Weering, T.C.E., 2009. Late Holocene (0–2.4 ka BP) surface water temperature and salinity variability, Feni Drift, NE Atlantic Ocean. Quat. Sci. Rev. 28, 1941–1955. http://dx.doi.org/10.1016/j.quascirev.2009.04.008.

Rodrigues, T., Grimalt, J.O., Abrantes, F.G., Flores, J.A., Lebreiro, S.M., 2009. Holocene interdependences of changes in sea surface temperature, productivity, and fluvial inputs in the Iberian continental shelf (Tagus mud patch). Geochem. Geophys. Geosyst 10, Q07U06. http://dx.doi.org/10.1029/2008GC002367.

Routson, C.C., Woodhouse, C.A., Overpeck, J.T., 2011. Second century megadrought in the Rio Grande headwaters, Colorado: How unusual was medieval drought? Geophys. Res. Lett. 38, L22703. http://dx.doi.org/10.1029/2011GL050015.

Rustic, G.T., Koutavas, A., Marchitto, T.M., Linsley, B.K., 2015. Dynamical excitation of the tropical Pacific ocean and ENSO variability by little ice age cooling. Science 350, 1537–1541. http://dx.doi.org/10.1126/science.aac9937.

Saenger, C., Cohen, A.L., Oppo, D.W., Halley, R.B., Carilli, J.E., 2009. Surface-temperature trends and variability in the low-latitude North Atlantic since 1552. Nat. Geosci. 2, 492–495. http://dx.doi.org/10.1038/ngeo552.

Schimmelmann, A., Hendy, I.L., Dunn, L., Pak, D.K., Lange, C.B., 2013. Revised ~2000-year chronostratigraphy of partially varved marine sediment in Santa Barbara Basin, California. GFF 135, 258–264. http://dx.doi.org/10.1080/11035897.2013.773066.

Schubert, S., Gutzler, D., Wang, H., Dai, A., Delworth, T., Deser, C., Findell, K., Fu, R., Higgins, W., Hoerling, M., Kirtman, B., Koster, R., Kumar, A., Legler, D., Lettenmaier, D., Lyon, B., Magana, V., Mo, K., Nigam, S., Pegion, P., Phillips, A., Pulwarty, R., Rind, D., Ruiz-Barradas, A., Schemm, J., Seager, R., Stewart, R., Suarez, M., Syktus, J., Ting, M., Wang, C., Weaver, S., Zeng, N., 2009. A U.S. CLIVAR project to assess and compare the responses of global climate models to drought-related SST forcing patterns: overview and results. J. Clim. 22, 5251–5272. http://dx.doi.org/10.1175/2009JCLI3060.1.

Seager, R., Kushnir, Y., Herweijer, C., Naik, N., Velez, J., 2005. Modeling of tropical forcing of persistent droughts and pluvials over western North America: 1856–2000. J. Clim. 18, 4065–4088. http://dx.doi.org/10.1175/JCLI3522.1.

Seager, R., Graham, N., Herweijer, C., Gordon, A.L., Kushnir, Y., Cook, E., 2007. Blueprints for medieval hydroclimate. Quat. Sci. Rev. 26, 2322–2336. http://dx.doi.org/10.1016/j.quascirev.2007.04.020.

Seager, R., Burgman, R., Kushnir, Y., Clement, A., Cook, E., Naik, N., Miller, J., 2008. Tropical Pacific forcing of North American medieval megadroughts: testing the concept with an atmosphere model forced by coral-reconstructed SSTs. J. Clim. 21, 6175–6190. http://dx.doi.org/10.1175/2008JCLI2170.1.

Seager, R., Goddard, L., Nakamura, J., Henderson, N., Lee, D.E., 2014. Dynamical causes of the 2010/11 Texas–Northern Mexico drought. J. Hydrometeor 15, 39–68. http://dx.doi.org/10.1175/JHM-D-13-024.1.

Sepúlveda, J., Pantoja, S., Hughen, K.A., Bertrand, S., Figueroa, D., León, T., Drenzek, N.J., Lange, C., 2009. Late Holocene sea-surface temperature and precipitation variability in northern Patagonia, Chile (Jacaf Fjord, 44°S). Quat. Res. 72, 400–409. http://dx.doi.org/10.1016/j.yqres.2009.06.010.

Sicre, M.-A., Yiou, P., Eiríksson, J., Ezat, U., Guimbaut, E., Dahhaoui, I., Knudsen, K.-L., Jansen, E., Turon, J.-L., 2008. A 4500-year reconstruction of sea surface temperature variability at decadal time-scales off North Iceland. Quat. Sci. Rev. 27, 2041–2047. http://dx.doi.org/10.1016/j.quascirev.2008.08.009.

Sicre, M.-A., Hall, I.R., Mignot, J., Khodri, M., Ezat, U., Truong, M.-X., Eiríksson, J., Knudsen, K.-L., 2011. Sea surface temperature variability in the subpolar Atlantic over the last two millennia. Paleoceanography 26, PA4218. http://dx.doi.org/10.1029/2011PA002169.

Spielhagen, R.F., Werner, K., Sørensen, S.A., Zamelczyk, K., Kandiano, E., Budeus, G., Husum, K., Marchitto, T.M., Hald, M., 2011. Enhanced modern heat transfer to the Arctic by warm Atlantic water. Science 331, 450–453. http://dx.doi.org/10.1126/science.1197397.

Stahle, D.W., Cook, E.R., Cleaveland, M.K., Therrell, M.D., Meko, D.M., Grissino-Mayer, H.D., Watson, E., Luckman, B.H., 2000. Tree-ring data document 16th century megadrought over North America. Eos Trans. AGU 81, 121–125. http://dx.doi.org/10.1029/00EO00076.

St. George, S., Meko, D.M., Cook, E.R., 2010. The seasonality of precipitation signals embedded within the North American Drought Atlas. Holocene. http://dx.doi.org/10.1177/0959683610365937.

Stott, L., Cannariato, K., Thunell, R., Haug, G.H., Koutavas, A., Lund, S., 2004. Decline of surface temperature and salinity in the western tropical Pacific Ocean in the Holocene epoch. Nature 431, 56–59. http://dx.doi.org/10.1038/nature02903.

Thomson, D.J., 1982. Spectrum estimation and harmonic analysis. Proc. IEEE 70, 1055–1096. http://dx.doi.org/10.1109/PROC.1982.12433.

Tierney, J.E., Oppo, D.W., Rosenthal, Y., Russell, J.M., Linsley, B.K., 2010. Coordinated hydrological regimes in the Indo-Pacific region during the past two millennia. Paleoceanography 25, PA1102. http://dx.doi.org/10.1029/2009PA001871.

Tootle, G.A., Piechota, T.C., Singh, A., 2005. Coupled oceanic-atmospheric variability and U.S. streamflow. Water Resour. Res. 41, W12408. http://dx.doi.org/10.1029/2005WR004381.

van Oldenborgh, G.J., Te Raa, L., Dijkstra, H., Philip, S., 2010. Frequency- or amplitude-dependent effects of the Atlantic meridional overturning on the tropical Pacific Ocean. In: Presented at the EGU General Assembly Conference Abstracts, p. 5755.

Wanamaker, A.D., Kreutz, K.J., Schöne, B.R., Pettigrew, N., Borns, H.W., Introne, D.S., Belknap, D., Maasch, K.A., Feindel, S., 2007. Coupled North Atlantic slope water forcing on Gulf of Maine temperatures over the past millennium. Clim. Dyn. 31, 183–194. http://dx.doi.org/10.1007/s00382-007-0344-8.

Wang, H., Mehta, V.M., 2008. Decadal variability of the Indo-Pacific Warm Pool and its association with atmospheric and oceanic variability in the NCEP–NCAR and SODA reanalyses. J. Clim. 21, 5545–5565. http://dx.doi.org/10.1175/2008JCLI2049.1.

Wang, S.-Y., Hipps, L., Gillies, R.R., Yoon, J.-H., 2014. Probable causes of the abnormal ridge accompanying the 2013–2014 California drought: ENSO precursor and anthropogenic warming footprint. Geophys. Res. Lett. 41 http://dx.doi.org/10.1002/2014GL059748, 2014GL059748.

Woodhouse, C.A., Overpeck, J.T., 1998. 2000 Years of drought variability in the central United States. Bull. Am. Meteor. Soc. 79, 2693–2714. http://dx.doi.org/10.1175/1520-0477(1998)079<2693:YODVIT>2.0.CO;2.

Woodhouse, C.A., Kunkel, K.E., Easterling, D.R., Cook, E.R., 2005. The twentieth-century pluvial in the western United States. Geophys. Res. Lett. 32, L07701. http://dx.doi.org/10.1029/2005GL022413.

Woodhouse, C.A., Russell, J.L., Cook, E.R., 2009. Two modes of North American Drought from instrumental and paleoclimatic data. J. Clim 22, 4336–4347. http://dx.doi.org/10.1175/2009JCLI2705.1.

Wu, W., Tan, W., Zhou, L., Yang, H., Xu, Y., 2012. Sea surface temperature variability in southern Okinawa Trough during last 2700 years. Geophys. Res. Lett. 39, L14705. http://dx.doi.org/10.1029/2012GL052749.

Yan, H., Sun, L., Wang, Y., Huang, W., Qiu, S., Yang, C., 2011. A record of the Southern Oscillation Index for the past 2,000 years from precipitation proxies. Nat. Geosci. 4, 611–614. http://dx.doi.org/10.1038/ngeo1231.

Zhao, M., Eglinton, G., Read, G., Schimmelmann, A., 2000. An alkenone (U37K′) quasi-annual sea surface temperature record (A.D. 1440 to 1940) using varved sediments from the Santa Barbara Basin. Org. Geochem. 31, 903–917. http://dx.doi.org/10.1016/S0146-6380(00)00034-6.